

Spike Dynamics in the Presence of Noise*

Chunyi Gai[†], David Iron[†], Theodore Kolokolnikov[†], and John Rumsey[†]

Abstract. We study the effect of noise on dynamics of a single spike for the classical Gierer–Meinhardt model on a finite interval. When spatio-temporal noise is introduced in the equation for the activator, we derive a stochastic ODE that describes the motion of a single spike on a slow time scale. The steady state is described by a density distribution for spike positions, obtained via the corresponding Fokker–Planck PDE. For sufficiently small noise level, the spike performs random fluctuations near the center of the domain. As noise level is increased, the spike can deviate from the domain center but remains effectively “trapped” within a certain subinterval that includes the center. For even larger noise levels, the spike starts to undergo large excursions that eventually collide with the domain boundary and temporarily trap the spike there. By reformulating this problem in terms of mean first passage time, we derive the expected time for the spike to collide with the boundary. Several new open problems are also presented.

Key words. reaction-diffusion systems, stochastic PDEs, stochastic ODEs, asymptotic reduction

AMS subject classifications. 60H10, 60H15, 82C31, 92Bxx

DOI. 10.1137/20M1312319

1. Introduction. The goal of this paper is to study the effect of noise on spike dynamics in reaction-diffusion systems. We concentrate on dynamics of a single spike for the Gierer–Meinhardt (GM) model, which is among the simplest reaction-diffusion systems that manifests complex patterns. It was first introduced in [3] to describe biological morphogenesis. One of the simplest versions the GM model—which still admits rich pattern-formation structure—is [3, 6, 20],

$$(1.1) \quad u_t = \varepsilon^2 u_{xx} - u + u^2/v, \quad 0 = v_{xx} - v + \frac{u^2}{\varepsilon}.$$

We impose Neumann boundary conditions on an interval $x \in [-L, L]$: $u_x = v_x = 0$ at $x = \pm L$. Here, u and v represent activator and inhibitor concentrations, respectively, and we make the standard assumption that the inhibitor diffuses much faster than the activator, that is, $\varepsilon \ll 1$.

A key feature of (1.1) is that in the limit of small activator diffusivity $\varepsilon \rightarrow 0$, the model can produce localized spike patterns [3, 4]. These spiky patterns have been subject to intensive study over the last two decades, and by now there is a large literature on formation and stability of these patterns. We refer the reader to books [14, 20] and references therein. More relevant to this work, once spikes form, they typically exhibit a slow motion which can be effectively characterized by a system of ODEs for spike positions coupled to an algebraic system describing spike heights [6, 5].

*Received by the editors January 13, 2020; accepted for publication (in revised form) October 25, 2020; published electronically December 15, 2020.

<https://doi.org/10.1137/20M1312319>

[†]Department of Mathematics and Statistics, Dalhousie University, Halifax, NS B3H3J5, Canada (Chunyi.Gai@dal.ca, iron@mathstat.dal.ca, tkolokol@gmail.com, johndrumsey@gmail.com).

While spike pattern formation and various instabilities for the deterministic GM model are by now well understood, much less is known about behavior of spike solutions in the corresponding stochastic mathematical model. Several recent studies have looked at the effect of noise on Turing bifurcations [16, 1] as well as phenomenological/numerical investigations [13, 18, 7, 9]. The effect of stochastic diffusivity in the GM model was analyzed in [21]. More recently, existence of solutions for stochastic a shadow GM system was established in [12, 22].

There are many ways to introduce noise. In this paper, we study the effect of introducing the noise in an equation for the *activator*. As we will show, this has a direct effect on the motion of spikes. For concreteness, let us assume that only the decay rate of the activator u is stochastic, although similar analysis works for other types of noise, some of which we discuss in section 5. By introducing the noise in the decay of u , (1.1) then becomes

$$(1.2) \quad u_t = \varepsilon^2 u_{xx} - u + u^2/v + \sigma u W \frac{\sqrt{dt}}{dt}, \quad 0 = v_{xx} - v + \frac{u^2}{\varepsilon}, \quad u_x = v_x = 0 \text{ at } x = \pm L.$$

Here, $W(x, t)$ is the spatio-temporal Gaussian white noise chosen to be consistent with numerics. We chose this type of noise because it is easy to implement numerically using finite differences: one simply adds an appropriate amount of noise at each meshpoint and at each timestep. A drawback is that the noise magnitude is related to the number of meshpoints N used, so that it needs to be normalized appropriately. Here, we define W to be

$$(1.3) \quad W(x, t) = \psi_0(t) + \sqrt{2} \sum_{m=1}^{(N-1)/2} \left(\psi_m(t) \cos\left(\frac{m\pi}{L} x\right) + \phi_m(t) \sin\left(\frac{m\pi}{L} x\right) \right),$$

where ψ_m, ϕ_m are independent standard normal distributions of mean zero and variance one. This definition is motivated in part as follows. When discretizing (1.3) using finite differences on a uniform mesh $\{x_k\}$ of size N , one obtains that $W(x_k, t)$ are independent normal variables, all with variance N . See Appendix A for detailed explanations as well as the MATLAB code for simulating (1.2).

Let us summarize our main findings, which are illustrated in Figure 1. As is well known [6, 5], in the absence of noise, the spike center x_0 drifts toward a center of the domain $x = 0$ on a slow time ($O(\varepsilon^2)$) scale. The reduced equation for the motion of a single spike consists of an ODE for the spike position. When the noise is turned on in the activator equation, it manifests as noise at the level of reduced equation for the spike motion. As a result, the reduced equation becomes a *stochastic* ODE (SODE). In section 2 we derive the following SODE which describes the motion for the spike center x_0 :

$$(1.4a) \quad dx_0 \sim -\frac{2 \sinh(2x_0)}{\cosh(2x_0) + \cosh(2L)} ds + \sigma^* \xi \sqrt{ds}; \quad s = \varepsilon^2 t,$$

Here, $\xi(s) = \mathcal{N}(0, 1)$ is a normal random variable and σ^* is the standard deviation, independent of space, given by

$$(1.4b) \quad \sigma^* = \sigma \left(\frac{L}{\varepsilon}\right)^{1/2} \sqrt{\frac{10}{7}}.$$

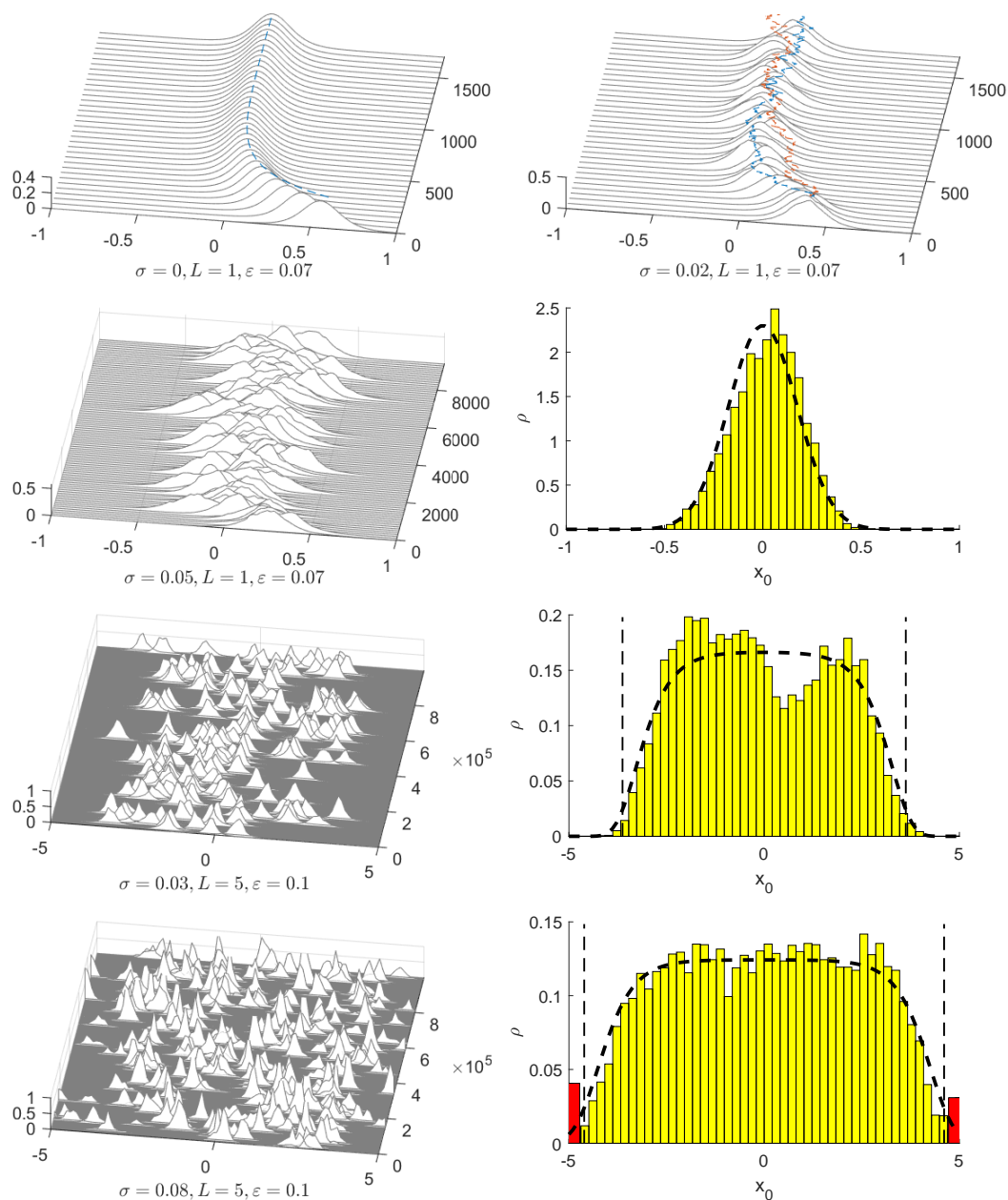


Figure 1. Top row and left column: simulation of the full PDE (1.2), parameters as indicated. Dashed lines correspond to the simulation of the SODE (1.4) for the reduced dynamics of the center of the spike. Right column, last three rows: histogram shows probability distribution of spike position over time, as extracted from the corresponding figure to its left. Dashed line denotes the analytical prediction (1.5). For larger σ (bottom right), the spike can hit the boundary and get “stuck” there for some time as indicated by red bars, then drift back to the middle.

The ODE (1.4a) is valid only as long as x_0 remains *away* from the boundaries $\pm L$, more specifically, as long as $|x_0 \pm L| \gg O(\varepsilon)$. In the absence of noise ($\sigma^* = 0$), the deterministic part pushes the spike toward its equilibrium at the center, while the noise can push it *away* from the center. If σ^* is relatively small, the deterministic part dominates, and the spike remains near the center of the domain. In this case, using the Fokker–Planck equation, and for sufficiently small σ^* , we show in section 3 that the stationary distribution of spike positions has the density given explicitly by

$$(1.5) \quad \rho(x_0) = C \exp \left\{ -\frac{2}{(\sigma^*)^2} \log \left(\frac{\cosh(2x_0) + \cosh(2L)}{1 + \cosh(2L)} \right) \right\},$$

where C is a constant chosen so that $\int \rho(x_0) dx_0 = 1$.

Figure 1 shows an excellent agreement of the direct simulations of (1.2) and the spike distribution density given by (1.5), (1.4b), as long as σ is not too big. Since the spike motion is restricted to the domain $[-L, L]$, formula (1.5) is restricted to those parameter values for which ρ is vanishingly small outside $x \in [-L, L]$.¹

On the other hand, when σ becomes too big, the density (1.5) does not “fit” into the domain $[-L, L]$ and there is a nonvanishing chance that a spike “hits” the boundary. While the SODE cannot predict what happens when the spike collides with the boundary, it can predict how long it takes (on average) before such collision occurs. Numerically, we observe that following the collision, the spike can remain at the boundary for some time, until the noise eventually kicks it off the boundary. This is illustrated in the bottom row of Figure 1; red bars correspond to the spike being temporarily “stuck” near the boundary. The expected time for the spike to “hit” the boundary can be formulated in terms of the mean first passage time (MFPT) problem. This is done in section 4.

We now summarize the paper. We derive the SODE (1.4) in section 2. The spike position distribution is analyzed in section 3; in the case of large L , we also derive the “trapping region” of size $2l$ such that the spike remains “trapped” within a region $|x| < l \leq L$. The hitting time to the boundary is studied in section 4. We conclude in section 5, where we discuss some generalizations and propose several open problems.

2. Derivation of reduced SODE for spike motion. We now derive the equations of motion (1.4) starting with the PDE system (1.2). In fact, we will generalize this slightly, by replacing

$$(2.1) \quad uW \rightarrow u^p W$$

in (1.2) and considering both the cases $p = 1$ and $p = 0$. A typical snapshot of solutions for the two cases is shown in Figure 2. The case $p = 0$ is discussed in section 5. When $p = 1$, the noise is mostly occurring inside a spike but does not affect the background due to exponential decay of u . On the other hand when $p = 0$, the noise affects the background and can lead to many other phenomena as discussed in section 5.

¹Here, “vanishing” is used loosely to mean exponentially small, meaning in practical terms that it is not expected to be observed numerically within a reasonable timeframe (say, a week of running on a standard laptop). For example, for parameters in row 2 of Figure 1, one finds $\rho(\pm L)/\rho(0) \approx 1.3 \times 10^{-10}$. The precise measure is clarified in section 4 in terms of MFPT.

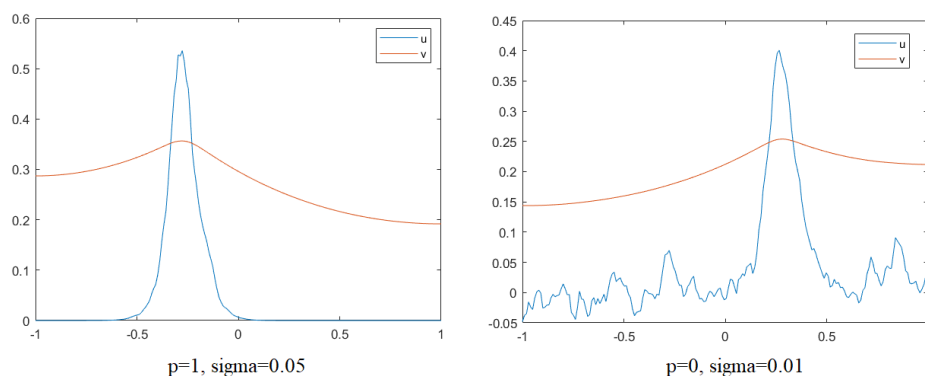


Figure 2. Spike in the presence of noise. Here, $\varepsilon = 0.05$. Left: when $p = 1$, the noise affects the inside of the spike only. Right: $p = 0$, the whole spike including the background is affected.

We use by-now-standard techniques to reduce the full PDE solution to an ODE system for spike center position x_0 . The derivation is rather standard; see, for example, [8, 6, 5, 11, 10, 19, 20]. In particular the deterministic part in (1.4) is well known, although we rederive it here in full for convenience. The main novelty here is to derive the reduced noise level σ^* (1.4b) from the original system.

Let $x_0(t)$ denote the position of the spike. In the inner region near x_0 we expand (1.2) as follows:

$$\begin{aligned} x &= x_0(s) + \varepsilon y, & s &= \varepsilon^2 t, \\ u(x, t) &= U_0(y) + \varepsilon U_1(y) + \dots, \\ v(x, t) &= V_0(y) + \varepsilon V_1(y) + \dots \end{aligned}$$

To leading order in ε we have

$$(2.2) \quad 0 = U_{0yy} - U_0 + \frac{U_0^2}{V_0}, \quad 0 = V_{0yy},$$

and at the next order, after collecting $O(\varepsilon)$ terms, we obtain

$$(2.3) \quad -x'_0(s)U_{0y} = U_{1yy} - U_1 + 2\frac{U_0U_1}{V_0} - \frac{U_0^2}{V_0^2}V_1 + \sigma U_0^p W \frac{\sqrt{ds}}{ds},$$

$$(2.4) \quad 0 = V_{1yy} + U_0^2.$$

Then V_0 is a constant and therefore U_0 can be written as

$$(2.5) \quad U_0(y) = w(y)V_0,$$

where w is the well-known ground state satisfying

$$(2.6) \quad w_{yy} - w + w^2 = 0, \quad w \rightarrow 0 \text{ as } |y| \rightarrow \infty, \quad w'(0) = 0,$$

with the explicit solution given by

$$(2.7) \quad w(y) = \frac{3}{2} \operatorname{sech}^2(y/2).$$

In the outer region, we write

$$(2.8) \quad v \sim SG(x, x_0),$$

where G is the Green's function satisfying

$$(2.9) \quad G_{xx} - G + \delta(x - x_0) = 0, \quad G_x(\pm L) = 0,$$

given by

$$(2.10) \quad G(x; x_0) = \frac{1}{\sinh(2L)} \begin{cases} \cosh(x+L) \cosh(x_0-L), & -L < x < x_0, \\ \cosh(x_0+L) \cosh(x-L), & x_0 < x < L, \end{cases}$$

and S is computed as

$$S = \int_{x_0^-}^{x_0^+} \frac{u^2(x)}{\varepsilon} dx \sim \int_{-\infty}^{\infty} (w(y)V_0)^2 dy = 6V_0^2.$$

Matching inner and outer regions we obtain $V_0 \sim v(x_0) \sim SG(x_0, x_0)$ so that

$$V_0 = \frac{1}{6G_0}; \quad G_0 = G(x_0, x_0) = \frac{\cosh(2x_0) + \cosh(2L)}{2 \sinh(2L)}.$$

Finally we formulate the solvability condition to determine x_0 . Multiplying (2.3) by U_{0y} we have

$$(2.11) \quad -x_0'(s) \int_{-\infty}^{\infty} U_{0y}^2 dy = \int_{-\infty}^{\infty} U_{0y} \left(U_{1yy} - U_1 + 2 \frac{U_0 U_1}{V_0} \right) dy \\ - \int_{-\infty}^{\infty} U_{0y} \frac{U_0^2}{V_0^2} V_1 dy + \sigma \frac{\sqrt{ds}}{ds} \int_{-\infty}^{\infty} U_{0y} U_0^p W dy.$$

We now integrate by parts using the decay of w at infinity to obtain

$$\int_{-\infty}^{\infty} U_{0y} \left(U_{1yy} - U_1 + 2 \frac{U_0 U_1}{V_0} \right) dy = \int_{-\infty}^{\infty} U_1 \left(U_{0yyy} - U_{0y} + 2 \frac{U_{0y} U_{0y}}{V_0} \right) dy.$$

Note that

$$U_{0yyy} - U_{0y} + 2 \frac{U_{0y} U_{0y}}{V_0} = (w_{yyy} - w_y + 2w w_y) V_0 = 0,$$

since $w_{yyy} - w_y + 2w w_y = (w_{yy} - w + w^2)_y = 0$ (see (2.6)). So (2.11) simplifies to

$$(2.12) \quad -x_0'(s) \int_{-\infty}^{\infty} U_{0y}^2 dy = - \int_{-\infty}^{\infty} U_{0y} \frac{U_0^2}{V_0^2} V_1 dy + \sigma \frac{\sqrt{ds}}{ds} \int_{-\infty}^{\infty} U_{0y} U_0^p W dy.$$

We further evaluate

$$(2.13) \quad - \int_{-\infty}^{\infty} U_{0y} \frac{U_0^2}{V_0^2} V_1 dy = \frac{V_0}{3} \int_{-\infty}^{\infty} w^3 V_{1y} dy.$$

From (2.4), we have

$$V_{1y}(y) = - \int_0^y U_0^2(s) ds + \frac{V_{1y}(\infty) + V_{1y}(-\infty)}{2}.$$

Since $\int_0^y U_0^2(s) ds$ is an odd function and using $\int_{-\infty}^{\infty} w^3 dy = \frac{36}{5}$, the integral in (2.13) evaluates to

$$\int_{-\infty}^{\infty} w^3 V_{1y} dy = \frac{V_{1y}(\infty) + V_{1y}(-\infty)}{2} \frac{36}{5}.$$

We match inner and outer solutions to obtain

$$V_{1y}(\pm\infty) = SG_x(x_0^\pm, x_0) = 6V_0^2 G_x(x_0^\pm, x_0).$$

Using $\int_{-\infty}^{\infty} w_y^2 dy = 6/5$ we get

$$(2.14) \quad x_0'(s) = - \frac{G_x(x_0^+, x_0) + G_x(x_0^-, x_0)}{G(x_0, x_0)} - \sigma \frac{\sqrt{ds}}{ds} V_0^{P-1} \frac{\int w_y w^p W dy}{6/5}.$$

From (2.10) we compute

$$(2.15) \quad \frac{G_x(x_0^+, x_0) + G_x(x_0^-, x_0)}{G(x_0, x_0)} = \frac{2 \sinh(2x_0)}{\cosh(2x_0) + \cosh(2L)}.$$

It remains to evaluate the integral in (2.14). Using the addition formulas $\cos(x) = \cos(x_0 + \varepsilon y) = \cos(x_0) \cos(\varepsilon y) - \sin(x_0) \sin(\varepsilon y)$ and parity, we compute

$$\begin{aligned} \int_{-\infty}^{\infty} w_y w^p \cos\left(x \frac{m\pi}{L}\right) dy &= -\sin\left(x_0 \frac{m\pi}{L}\right) \int_{-\infty}^{\infty} \sin\left(\varepsilon y \frac{m\pi}{L}\right) w_y w^p dy, \\ \int_{-\infty}^{\infty} w_y w^p \sin\left(x \frac{m\pi}{L}\right) dy &= \cos\left(x_0 \frac{m\pi}{L}\right) \int_{-\infty}^{\infty} \sin\left(\varepsilon y \frac{m\pi}{L}\right) w_y w^p dy. \end{aligned}$$

Define

$$F_p(x) := \int_{-\infty}^{\infty} \sin(xy) w_y w^p dy,$$

whose value is derived explicitly in Appendix B. In terms of F_p we have

$$(2.16) \quad \int W w_y w^p dy = \sqrt{2} \sum_{m=1}^{(N-1)/2} F_p\left(\frac{m\pi}{L} \varepsilon\right) \left(-\psi_m(t) \sin\left(x_0 \frac{m\pi}{L}\right) + \phi_m(t) \cos\left(x_0 \frac{m\pi}{L}\right)\right).$$

Finally, we compute the variance of $\sigma V_0^{P-1} \frac{\int w_y w^p W dy}{6/5}$. This is done by approximating the summation by an integral as follows:

$$\begin{aligned}
(\sigma^*)^2 &= \left(\frac{\sigma V_0^{P-1}}{6/5}\right)^2 2 \sum_{m=1}^{(N-1)/2} F_p^2\left(\frac{m\pi}{L} \varepsilon\right) \\
&\sim \left(\frac{\sigma V_0^{P-1}}{6/5}\right)^2 2 \int_0^{N/2} F_p^2\left(\frac{m\pi}{L} \varepsilon\right) dm \\
&\sim \left(\sigma G_0^{1-p} 5 \cdot 6^{-p}\right)^2 2 \frac{L}{\pi \varepsilon} \int_0^\infty F_p^2(z) dz.
\end{aligned}$$

The latter integral is computed in Appendix B with the result

$$\int_{-\infty}^\infty F_p^2(x) dx = \begin{cases} \frac{6}{5}\pi, & p = 0, \\ \frac{36}{35}\pi, & p = 1. \end{cases}$$

To summarize, we obtain

$$(2.17) \quad \sigma^* = \sigma \sqrt{\frac{L}{\varepsilon}} G_0^{1-p} C_p,$$

where

$$C_p = \sqrt{(5 \cdot 6^{-p})^2 \frac{2}{\pi} \int_0^\infty F_p^2(z) dz} = \begin{cases} \sqrt{\frac{60}{7}}, & p = 0, \\ \sqrt{\frac{10}{7}}, & p = 1. \end{cases}$$

In particular,

$$(2.18) \quad p = 0: \quad \sigma^* = \sigma \sqrt{\frac{15L}{\varepsilon}} \frac{\cosh(2x_0) + \cosh(2L)}{\sinh(2L)},$$

$$(2.19) \quad p = 1: \quad \sigma^* = \sigma \sqrt{\frac{L}{\varepsilon}} \sqrt{\frac{10}{7}}.$$

This yields (1.4) when $p = 1$. The case $p = 0$ is discussed in section 5.

A similar derivation is possible if we impose periodic boundary conditions on (1.2) instead of Neumann. Then the resulting ODE for spike motion is simply (1.4) but without the drift, $dx_0 \sim \sigma^* \xi \sqrt{ds}$, and with $x_0 \in [-L, L]$ taken mod $2L$ (so that the spike that crosses through a left boundary reemerges on the right and vice versa). This corresponds to a simple Brownian motion with periodic boundary conditions.

3. Spike position distribution.

For a general SODE

$$(3.1) \quad dx = f(x)ds + \sigma(x)\xi\sqrt{ds},$$

subject to initial condition $x(0) = a$, the probability density $\rho(x, t)$ for x to be at a given location at time t satisfies the Fokker–Planck PDE

$$\rho_t = \left(\frac{\sigma^2}{2}\rho\right)_{xx} - (f\rho)_x$$

subject to initial conditions $\rho(x, 0) = \delta(x - a)$. See, for example, [2, 15] for the derivation, or the appendix of [17] for an alternative derivation using integral master equation. The long-time equilibrium density distribution $\rho(x, t) = \rho(x)$ then satisfies $(\frac{\sigma^2}{2}\rho)_x + f\rho = K$. Assuming the density is finite and decays at $x = \pm\infty$, we must have $K = 0$ so that the equilibrium density is explicitly given by

$$(3.2) \quad \rho = \frac{2}{\sigma^2} C \exp\left(\int \frac{2}{\sigma^2} f\right),$$

where C is a constant of integration chosen so that $\int \rho = 1$. Here, we specialize to SODE (1.4). For convenience we relabel $x_0 = x$. We evaluate $\int_0^x f = -\log\left(\frac{\cosh(2x) + \cosh(2L)}{1 + \cosh(2L)}\right)$ and $\sigma(x) = \sigma^*$ is a constant. This leads to (1.5) for the density. In the context of a bounded domain $x \in [-L, L]$, this formula implicitly assumes that ρ is vanishingly small near $x = \pm L$. Figure 3 shows the graph of $\rho(x)$ for several values of L and σ^* . In the limit of small σ^* , the density is nearly Gaussian. By Taylor-expanding (1.5) for small x we obtain

$$(3.3) \quad \rho(x_0) \sim C \exp\left\{-\frac{1}{(\sigma^*)^2} \frac{4x^2}{1 + \cosh(2L)}\right\},$$

where $C = \sqrt{\frac{1}{\pi} \frac{1}{(\sigma^*)^2} \frac{4}{1 + \cosh(2L)}}$.

On the other hand, when $L \gg 1$, (1.5) simplifies to

$$(3.4) \quad \rho(x) = C \exp\left\{-\frac{2}{(\sigma^*)^2} e^{2(|x|-L)}\right\}.$$

As shown in Figure 3, this is well-approximated by a piecewise-constant density. $\rho \sim \frac{1}{2l} \chi_{[-l, l]}$, where χ is the characteristic function. The length l of the box can be computed by setting $\rho(l) = a\rho(0)$, where $0 < a < 1$ is an arbitrarily chosen constant. Solving for l then yields

$$l \sim L - \log\left(\frac{1}{\sigma^*} \sqrt{\frac{2}{\log a^{-1}}}\right).$$

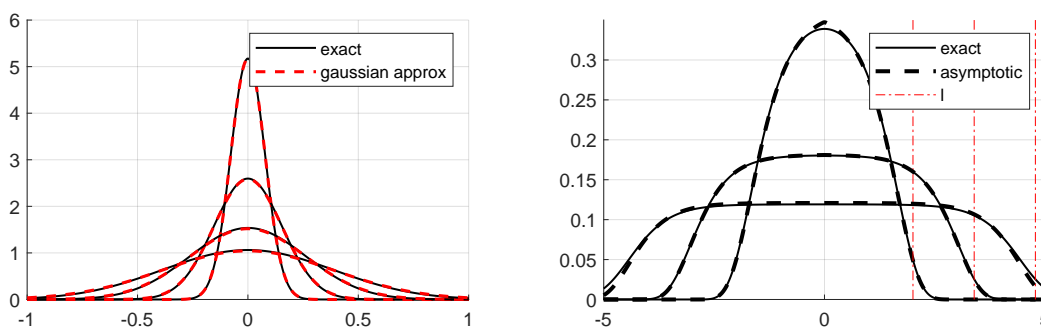


Figure 3. Spike density distribution $\rho(x)$ for several values of σ^* and L . Left: $L = 1$ and $\sigma^* = 0.1, 0.2, 0.3, 0.5$ (from highest to lowest). Solid line is the exact formula (1.5), whereas dashed line is the formula (3.3). Right: $L = 5$ and $\sigma^* = 0.1, 0.2, 0.3, 0.5$ (from highest to lowest). Solid line is the exact formula (1.5), whereas dashed line is the formula (3.4).

The choice of a is somewhat subjective. For sufficiently small σ^* (with $(\sigma^*)^2 \ll O(\log a^{-1})$), to leading order we get

$$(3.5) \quad l \sim L - \log \frac{1}{\sigma^*}.$$

This formula is shown in Figure 3 (right); it also corresponds to choosing $a = e^{-2}$.

When $1 \ll l \ll L$, $\rho(x)$ exhibits a sharp transition near $x \sim l$: for $|x| \ll l$, we find $\rho(x) \sim C$ so that $\rho(x)$ is nearly constant in this case. For $l \ll |x| \leq L$, $\rho(x)$ is exponentially small so that $\rho(x)$ is nearly zero in that region. On the other hand, when l is near L , the density is nonnegligible near $x = L$ and the spike is no longer confined away from the boundaries $\pm L$. In this case it will hit the boundary within a realistic timeframe (i.e., observable numerically on a computer for runtimes less than, e.g., a week). In the next section, we use MFPT to quantify this transition more precisely.

4. Boundary hitting time. As seen from SODE (1.4), the spike motion is driven by a competition between the deterministic term that pushes the spike toward the center of the domain and the noise term which can push the spike away from the center. If the noise is sufficiently large, it can counteract the attraction toward the center, and the spike will eventually collide with the boundary, given enough time.

We can formulate this as the MFPT, corresponding to a stochastic particle first hitting the boundary $x = \pm L$. Consider the general SODE,

$$(4.1) \quad dx = f(x)ds + \sigma^* \xi \sqrt{ds},$$

and let $m(x)$ be the average time it takes for a particle x to hit the boundary $x = \pm L$. Then $m(x)$ satisfies the following MFPT problem [15]:

$$(4.2) \quad \frac{(\sigma^*)^2}{2} m_{xx} + f(x)m_x + 1 = 0, \quad m(\pm L) = 0.$$

An alternative derivation from first principles is given in Appendix C. For our problem,

$$(4.3) \quad f(x) = -\frac{2 \sinh(2x)}{\cosh(2x) + \cosh(2L)}$$

and the solution to (4.2) is given by

$$(4.4) \quad m_x = -\frac{2}{(\sigma^*)^2} v_h \int_0^x \frac{1}{v_h(s)} ds,$$

where v_h satisfies $\frac{(\sigma^*)^2}{2} v_h' + f(x)v_h = 0$, that is,

$$(4.5) \quad v_h(x) = \exp\left(-\frac{2}{(\sigma^*)^2} \int_0^x f(s) ds\right).$$

Integrating (4.4) and using the boundary condition $m(L) = 0$ yields a semiexplicit expression for MFPT,

$$(4.6) \quad m(x) = \frac{2}{(\sigma^*)^2} \int_x^L \left\{ v_h(x) \int_0^x \frac{1}{v_h(s)} ds \right\} dx.$$

Further analysis is possible for two important cases: either L is large, or σ is small (or both).

Case A: σ^* is small and $L = O(1)$. We use Laplace's method to asymptotically approximate $m(x)$. Note that $f(x)$ is a decreasing function so that $\int_0^x f$ has a maximum at $x = 0$. Therefore we estimate, using Laplace's method, for $x > 0$,

$$\int_0^x \frac{1}{v_h(s)} ds \sim \int_0^\infty \exp\left(\frac{2}{(\sigma^*)^2} \int_0^x f(s) ds\right) dx \sim \frac{\sigma^*}{2} \sqrt{\frac{\pi}{-f'(0)}}$$

so that

$$m(x) \sim \frac{1}{\sigma^*} \sqrt{\frac{\pi}{-f'(0)}} \int_x^L \exp\left(-\frac{2}{(\sigma^*)^2} \int_0^x f(s) ds\right) dx.$$

Note that $-\int_0^x f$ attains its maximum at $|x| = L$ so we estimate, for $x > 0$,

$$(4.7) \quad \int_x^L \exp\left(-\frac{2}{(\sigma^*)^2} F(x)\right) dx \sim \exp\left(-\frac{2}{(\sigma^*)^2} \int_0^L f(s) ds\right) \frac{(\sigma^*)^2}{2(-f(L))} \left(1 - \exp\left(-\frac{2f(L)}{(\sigma^*)^2}(x-L)\right)\right).$$

For $x < 0$, we simply replace x by $|x|$ in (4.7) since $m(x)$ is symmetric. To summarize, we obtain the following uniformly valid expression when $\sigma^* \ll 1$:

$$(4.8) \quad m(x) \sim \left(1 - \exp\left(-\frac{2f(L)}{(\sigma^*)^2}(|x| - L)\right)\right) m_{\max}, \text{ where}$$

$$(4.9) \quad m_{\max} = \frac{\sigma^*}{2(-f(L))} \sqrt{\frac{\pi}{-f'(0)}} \exp\left(-\frac{2}{(\sigma^*)^2} \int_0^L f(s) ds\right).$$

Specializing to (4.3) we obtain after some algebra,

$$(4.10a) \quad m(x) \sim \left(1 - \exp\left(\frac{2 \tanh(2L)}{(\sigma^*)^2}(|x| - L)\right)\right) m_{\max}, \quad \sigma^* \rightarrow 0,$$

$$(4.10b) \quad m_{\max} = \sqrt{2\pi} \frac{\cosh(2L)}{8 \sinh(2L)} \sigma^* \exp\left\{\frac{2}{\sigma^*} \log(1 + \tanh^2 L)\right\}.$$

As can be seen from (4.10b), m_{\max} increases exponentially as $\sigma^* \rightarrow 0$.

Case B: Large L . We estimate, for $x > 0$,

$$f(x) \sim -\frac{2}{1 + e^{2L-2x}}$$

and in particular $f(x) \sim 0$ for $|x| \ll L$. We then estimate

$$\int_0^x f(x) \sim -\log(1 + e^{2(x-L)}) \sim \begin{cases} 0, & x \ll L, \\ -\log(2) + -(x-L), & x \text{ near } L. \end{cases}$$

This yields the following uniform expansion for v_h :

$$v_h = \exp \left[\frac{2 \log(1 + e^{2(x-L)})}{(\sigma^*)^2} \right] \sim 1 + \exp \left(\frac{2 \log(2)}{(\sigma^*)^2} \right) \exp \left(\frac{2}{(\sigma^*)^2} (x - L) \right).$$

We then estimate, for $x > 0$,

$$\int_0^x \frac{1}{v_h(s)} ds \sim x$$

and

$$\begin{aligned} \int_x^L \left\{ v_h(x) \int_0^x \frac{1}{v_h(s)} ds \right\} dx &\sim \int_x^L \{v_h(x)x\} dx \\ &\sim \int_x^L x dx + \int_x^L \exp \left(\frac{2 \log(2) + 2(x-L)}{(\sigma^*)^2} \right) L dx \\ &\sim \frac{L^2 - x^2}{2} + \exp \left(\frac{2 \log(2)}{(\sigma^*)^2} \right) \frac{(\sigma^*)^2}{2} L \left\{ 1 - \exp(2(x-L)/(\sigma^*)^2) \right\}. \end{aligned}$$

In conclusion, we obtain

$$(4.11) \quad m(x) \sim \frac{L^2 - x^2}{(\sigma^*)^2} + \exp \left(2 \frac{\log(2)}{(\sigma^*)^2} \right) L \left\{ 1 - \exp(2(|x| - L)/(\sigma^*)^2) \right\}$$

and in particular

$$(4.12) \quad m(0) \sim \frac{L^2}{(\sigma^*)^2} + 2 \exp \left(\frac{2 \log(2)}{(\sigma^*)^2} \right) L, \quad L \gg O(1).$$

Formula (4.12) is shown in Figure 4 (top right). Note the parabolic shape on top of an exponential layer, as predicted by the asymptotics (4.11).

While $m(x)$ gives the mean of the hitting time distribution, the distribution itself does not concentrate around the mean. Figure 4 (bottom) shows the hitting time probability distribution obtained using Monte Carlo simulations. We simulated (1.4) 10,000 times starting with $x(0) = 0$, until x collided with a boundary $x = \pm L$. The time of collision for each simulation is recorded, and the resulting histogram is shown. The value of $m(0)$ is approximated by the average of these simulations. In Figure 4, bottom left, we used forward Euler with $ds = 10^{-3}$ in the simulations. The average of these simulations is $m_{Monte-Carlo}(0) = 23.1$. Exact result (4.6) gives $m_{exact}(0) = 21.97$, whereas asymptotic result (4.10a) is $m_{asympt}(0) = 19.48$, a 13% difference. In Figure 4, bottom right, we used $ds = 10^{-2}$ and obtained $m_{Monte-Carlo}(0) = 1429$. Exact result (4.6) gives $m_{exact}(0) = 1203.7$, whereas asymptotic result (4.12) yields $m_{asympt}(0) = 1380$, a 15% difference. Overall, a good agreement between exact result, Monte Carlo, and asymptotics is observed.

The error between m_{exact} and $m_{Monte-Carlo}$ depends on the number N of simulations used. While the error analysis is outside the scope of this paper, numerics indicate that it scales like $O(1/\sqrt{N})$, which is typical of Monte Carlo simulations in general. The error between m_{exact} and $m_{Monte-Carlo}$ depends on both σ^* and L in a complex way depending on the relative scaling of L and σ^* . Numerics indicate that with σ^* fixed, formula (4.12) has a relative error of $O(1/L)$ as $L \rightarrow \infty$, whereas formula (4.10) has a relative error that decays exponentially in σ^* for fixed L and with $\sigma^* \rightarrow 0$.

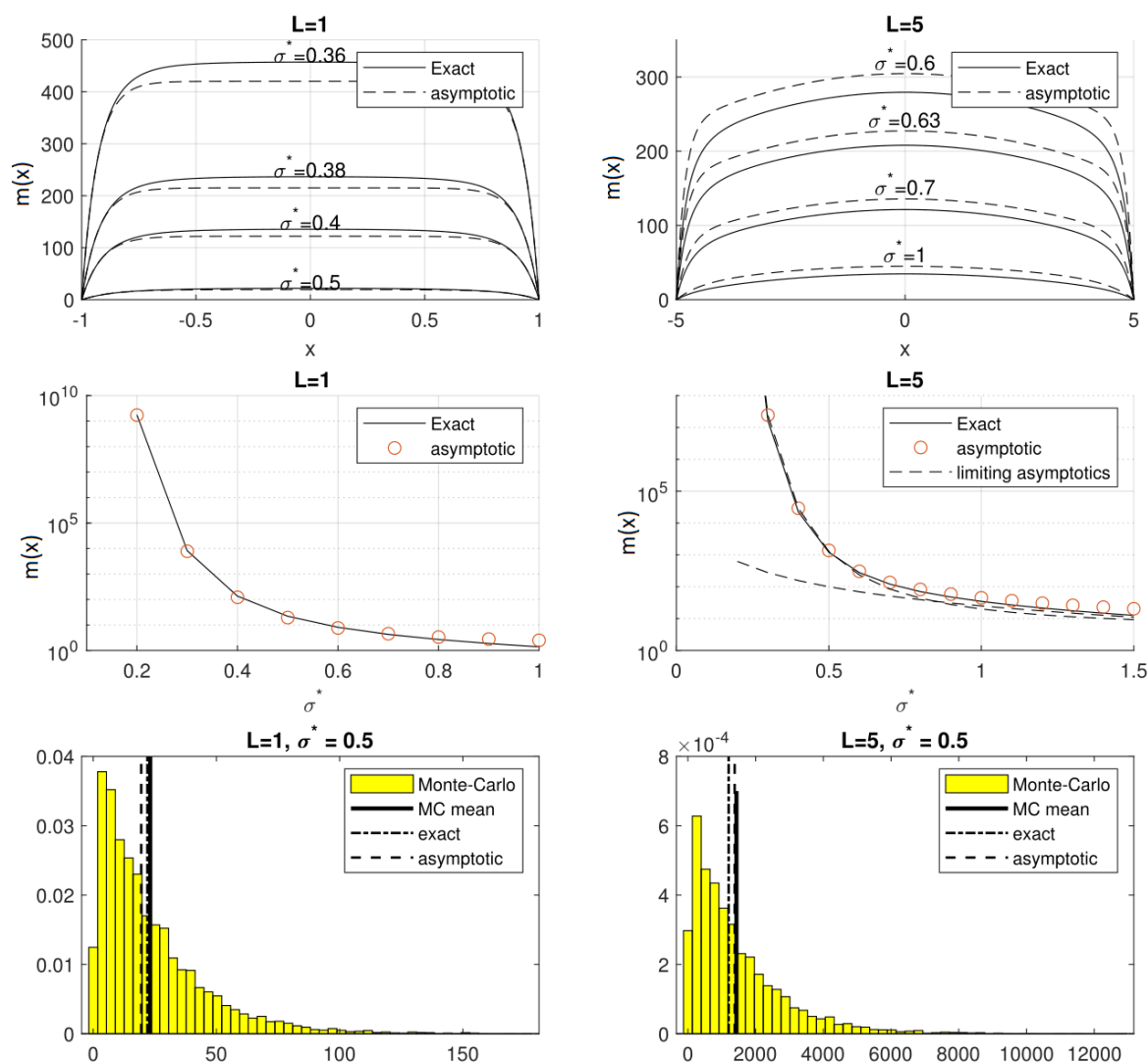


Figure 4. Top row: FPT $m(x)$ for $L = 1$ and $L = 10$ for several σ^* as shown. Note the parabolic profile on top of an exponential layer when $L = 5$ and $\sigma \geq 0.5$. Middle row: graph of $m(0)$ for $L = 1$ and $L = 5$ as a function of σ^* . Bottom row: the full distribution of hitting times obtained by Monte Carlo simulations of (1.4a). MC-mean refers to the average of these simulations. Exact result is $m(0)$ given by (4.6). Asymptotic line is given by (4.10a) for $L = 1$ and by (4.11) for $L = 5$.

5. Discussion. We have investigated the effect of noise on the motion of a single spike in the GM model. We formulated a SODE describing the reduced spike motion, then used it to describe the spike distribution of a spike inside the domain and the MFPT for the spike to hit the boundary. This only scratches the surface of many novel phenomena that are possible when noise is present, and many open problems remain. We conclude with proposing several below.

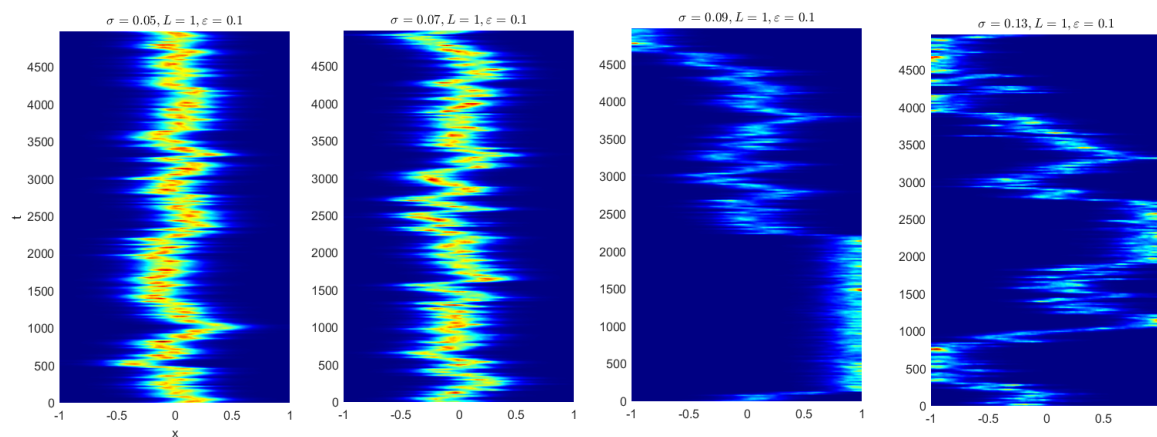


Figure 5. Simulation of (1.2) for several different σ as indicated. As σ is increased, the spike collides with the boundary. It can stay at the boundary for a long time but eventually becomes “unglued.” The higher the σ , the shorter time it spends at the boundary. The spike still retains its shape even for larger σ .

When a spike hits the boundary, it gets “stuck” there. However, it can also get “unglued” from the boundary as well, as illustrated in Figure 5. While we used MFPT theory to predict how long it takes for the spike to “hit” the boundary, we cannot explain why it gets “unglued” or how long it takes for the spike to unglue.

In this paper, we added the noise to the activator equation because it induces random spike motion. Numerical experiments indicate that noise in the inhibitor does not affect spike motion very much; instead, it induces spike oscillations. This is an interesting problem left for future study.

We studied in detail multiplicative noise (1.2), where the spatiotemporal noise is premultiplied by u . This type of noise ensures that the randomness affects only the spike itself and has no effect outside the spike, since u decays exponentially away from the spike center. One can also consider additive noise, where the noise is added to the background independent of spike height, as follows:

$$(5.1) \quad \begin{cases} u_t = \varepsilon^2 u_{xx} - u + u^2/v + \sigma W \frac{\sqrt{dt}}{dt}, & 0 = v_{xx} - v + \frac{u^2}{\varepsilon}, \\ u_x = v_x = 0 \text{ at } x = \pm L. \end{cases}$$

Using the analysis of section 2, the spike position then satisfies the SODE (1.4), with σ^* given by (2.19). The resulting density distribution, as derived in (3.2), is given by

$$\rho = \frac{C}{(\cosh(2x_0) + \cosh(2L))^2} \exp\left(-\frac{\varepsilon}{15L\sigma^2} \frac{\sinh^2(2L)}{(\cosh(2x_0) + \cosh(2L))^2}\right).$$

It is qualitatively similar to the multiplicative case (1.5). The difference is that adding background noise affects not just the spike motion but spike stability as well—something that reduced SODE or density (5.1) does not capture, especially in the case of multiple spikes. Figure 6 shows simulations for different levels of additive noise and domain size. Many new phenomena are observed, including spike death, spike insertion, and “switching” behavior. These are great open problems left for future study.

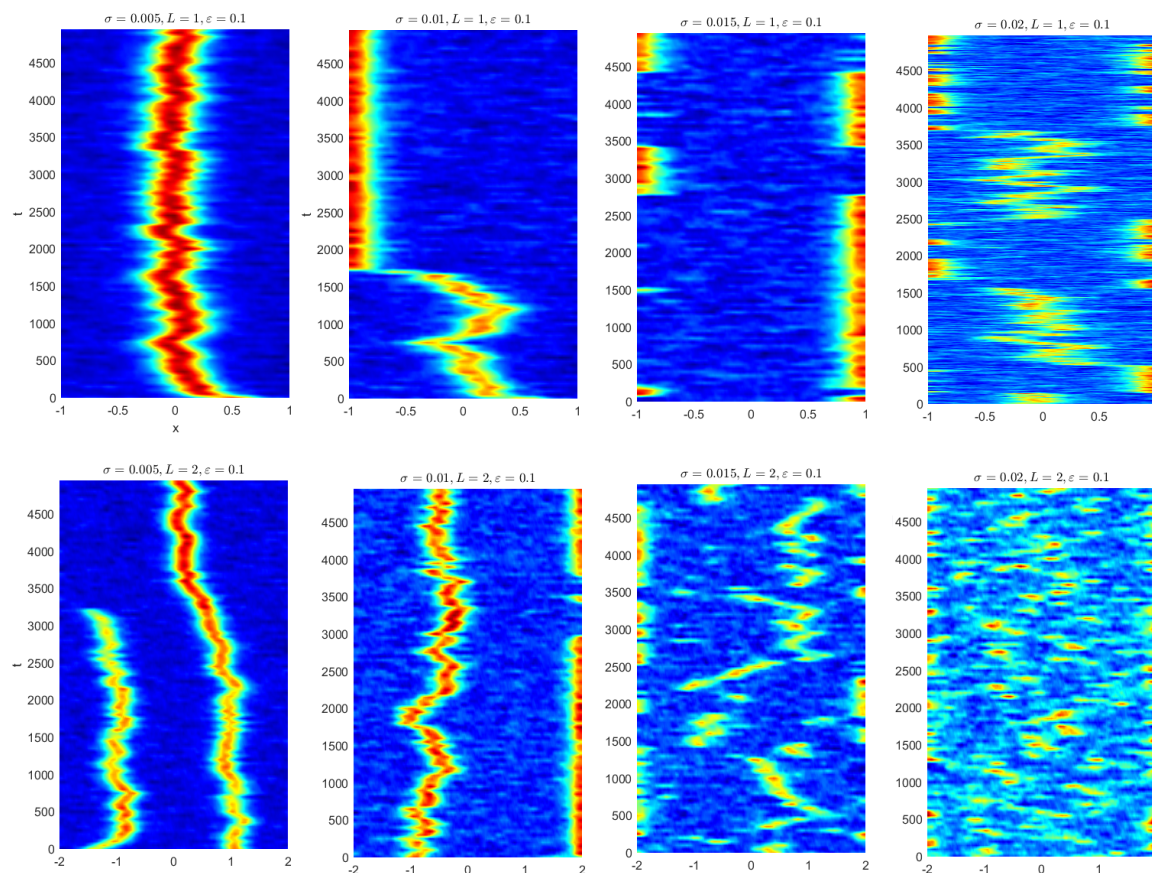


Figure 6. Simulation of (5.1) for two different domain sizes and various σ as indicated. Depending on domain length and noise level, many interesting phenomena are observed including boundary switching (top row, panel 3), spike death (bottom row, left), and chaotic dynamics (bottom right).

Appendix A: Numerical method. We use finite differences to solve (1.2) numerically.

Discretize in space using N gridpoints, $\Delta x = 2L/N$, and in time using stepsize Δt so that $u(x_k, t_j) \approx w_j^k$, $v(x, t) \approx n_j^k$, where $x_k = -L + \Delta x k$ with $k = 1 \dots N$, $t_j = \Delta t j$. We use a simple implicit-explicit finite differences scheme, similar to what is described in [1]. Laplacian is discretized implicitly, the rest explicitly. This results in

$$\frac{u_{j+1}^k - u_j^k}{\Delta t} = \varepsilon^2 \frac{u_{j+1}^{k+1} + u_{j+1}^{k-1} - 2u_{j+1}^k}{(\Delta x)^2} - u_{j+1}^k + \frac{(u_j^k)^2}{v_j^k} + \sigma \frac{\sqrt{\Delta t}}{\Delta t} W_j^k,$$

$$0 = \mu^2 \frac{v_{j+1}^{k+1} + v_{j+1}^{k-1} - 2v_{j+1}^k}{(\Delta x)^2} - v_j^k + \frac{(u_j^k)^2}{\varepsilon}.$$

Neumann boundary conditions are implemented by assuming $u_{j+1} = u_{j-1}$ when $j = 1$ or N , and similarly for v .

Here, W_j^k is the discretization of the noise term. To compute W_j^k , note that $W(x, t)$ is normally distributed with zero mean (since it is a sum of normal variables). Moreover, we have

$$\mathcal{E} \{W(x_k, t)W(x_l, t)\} = \begin{cases} 0 & \text{if } k \neq l, \\ N & \text{if } k = l. \end{cases}$$

This follows from the fact that $\mathcal{E} \{\phi_k \phi_l\} = \mathcal{E} \{\psi_k \psi_l\} = \delta_{kl}$; $\mathcal{E} \{\phi_k \psi_l\} = 0$; and identities

$$\begin{aligned} \sum_{m=1}^{(N-1)/2} \cos\left(\frac{2\pi}{N}ml\right) \cos\left(\frac{2\pi}{N}mk\right) &= \left(\frac{N}{4} - 1\right) \delta_{l,k}, & \sum_{m=1}^{(N-1)/2} \sin\left(\frac{2\pi}{N}ml\right) \sin\left(\frac{2\pi}{N}mk\right) &= \frac{N}{4} \delta_{l,k}, \\ \sum_{m=1}^{(N-1)/2} \sin\left(\frac{2\pi}{N}mj\right) \cos\left(\frac{2\pi}{N}mk\right) &= 0. \end{aligned}$$

Therefore W_j^k , $k = 1 \dots N$, are N independent normally distributed variables with mean zero and standard deviation \sqrt{N} . In MATLAB language, such a random variable is generated using the command `sqrt(N)*randn`. Figure 7 illustrates the code for this.

Appendix B: Some integrals. 1. Evaluation of $F_p(x) = \int_{-\infty}^{\infty} \sin(xy)w^p w_y dy$ with $p = 0$. Integrating by parts we have

$$F_0(x) = -x \int_{-\infty}^{\infty} \cos(xy)w(y)dy = -6x \operatorname{Re} \left(\int_{-\infty}^{\infty} \frac{e^{ixy}}{(e^{y/2} + e^{-y/2})^2} dy \right).$$

The integrand has residues at $y = i\pi(1+2n)$, $n \in \mathbb{Z}$. A standard computation of a second-order residue yields

$$\operatorname{Res}_{y=i\pi} \frac{e^{ixy}}{(e^{y/2} + e^{-y/2})^2} = -ixe^{-\pi x}.$$

Consider a rectangular contour C traversed counterclockwise whose base C_1 is the x -axis, whose height C_2 is at $y = i2\pi$, and whose left and right sides go to $\pm\infty$. Then

$$\int_{C_1} \frac{e^{ixy}}{(e^{y/2} + e^{-y/2})^2} dy = I; \quad \int_{C_2} \frac{e^{ixy}}{(e^{y/2} + e^{-y/2})^2} dy = -e^{-2\pi x} I$$

so that $I - e^{-2\pi x} I = 2\pi x e^{-\pi x}$ or $I = \frac{\pi x}{\sinh(\pi x)}$. This yields

$$(5.2) \quad F_0(x) = \frac{-6\pi x^2}{\sinh(\pi x)}.$$

2. Evaluation of $F_p(x)$ with $p = 1$. Integrating by parts we have

$$\begin{aligned} F_1 &= -\frac{x}{2} \int_{-\infty}^{\infty} \cos(xy)w^2 dy = -\frac{x}{2} \int_{-\infty}^{\infty} \cos(xy) (w - w'') dy \\ &= -\frac{x}{2} \int_{-\infty}^{\infty} \cos(xy) (1 + x^2) w dy = \frac{(1 + x^2)}{2} F_0(x). \end{aligned}$$

```

L=1; sigma=0.1; eps=0.1;
N=200; dt=0.1;
x=linspace(-L,L,N)'; dx=x(2)-x(1);

Lap=-2*diag(ones(1,N))+diag(ones(1,N-1),1)+diag(ones(1,N-1),-1);
Lap(1,2)=2;Lap(N,N-1)=2; Lap=Lap/dx^2;
Id=eye(N);
M1=Id-eps^2*Lap*dt;
M2=Id-Lap;

v=x*0+1; u=sech((x-L*0)/eps);
tout=0;
for t=0:dt:4000
    noise=randn(N,1)*sqrt(N)*sigma;
    rhs1=u+(-u+u.^2./v)*dt+noise.*u*sqrt(dt);
    rhs2=u.^2./eps;

    u=M1\rhs1;
    v=M2\rhs2;

    if t>tout
        tout=tout+10;
        plot(x,u,x,v);
        legend('u','v');xlabel('x');
        title(sprintf('t=%g eps=%g',t,eps));
        drawnow;
    end;
end;

```

Figure 7. Code for simulating (1.2). Copy and paste into MATLAB to run.

This yields

$$(5.3) \quad F_1(x) = \frac{-3\pi(x^2 + x^4)}{\sinh(\pi x)}.$$

3. Evaluation of $\int_0^\infty (F_p(x))^2 dx$. We first evaluate the integrals

$$I_K = \int_0^\infty \frac{x^K}{(e^{\pi x} - e^{-\pi x})^2}, \quad K = 2, 4, 6, 8.$$

We have

$$\frac{x^{2K}}{(e^{\pi x} - e^{-\pi x})^2} = \frac{x^K e^{-2\pi x}}{(1 - e^{-2\pi x})^2} = \sum_{n=1}^{\infty} x^K e^{-2\pi x n}$$

and recalling that $\int_0^\infty x^K e^{-sx} dx = \Gamma(K+1)s^{-K-1}$ we obtain

$$I_K = \Gamma(K+1) (2\pi)^{-K-1} \sum_{n=1}^{\infty} n^{-K}.$$

The sum above is the zeta function whose values for even K are well known (see Wikipedia). In particular this yields

$$I_2 = \frac{1}{24\pi}, \quad I_4 = \frac{1}{120\pi}, \quad I_6 = \frac{1}{168\pi}, \quad I_8 = \frac{1}{120\pi}.$$

Finally we get

$$(5.4) \quad \int_0^\infty (F_0(x))^2 dx = 144\pi^2 I_4 = \frac{6}{5}\pi;$$

$$(5.5) \quad \int_0^\infty (F_1(x))^2 dx = 36\pi^2 (I_8 + 2I_6 + I_4) = \frac{36}{35}\pi.$$

Appendix C: Derivation of the MFPT equation. Here, we derive the formula for MFPT from the first principles. Suppose we are given a SODE with variable drift and noise:

$$dx = f(x)dt + \sigma(x)\sqrt{dt}\xi.$$

The following integral equation gives MFPT:

$$(5.6) \quad u(x) = dt + \int_{-\infty}^{\infty} \frac{\exp\left(-\frac{(x-y)^2}{2\sigma^2(x)dt}\right)}{\sqrt{2\pi dt}\sigma(x)} u(y + f(x)dt) dy.$$

It states that MFPT at location x can be computed by looking at MFPT at all other locations y , taking a deterministic jump $f(x)dt$, then taking a stochastic jump weighted by the probability of getting from y to x .

Perform a change of variables, $y = x + z\sqrt{2\sigma^2(x)dt}$, so that (5.6) becomes

$$(5.7) \quad u(x) = dt + \int_{-\infty}^{\infty} \frac{\exp(-z^2)}{\sqrt{\pi}} u(x + \varepsilon z + \varepsilon^2 b) dz, \quad \text{where } \varepsilon = \sqrt{2\sigma^2(x)dt}, \quad b = \frac{f(x)}{2\sigma^2(x)}.$$

We further expand

$$u(x + z\varepsilon + \varepsilon^2 b) = u(x) + \varepsilon z u_x + \varepsilon^2 \left(b u_x + \frac{z^2}{2} u_{xx} \right) + \dots$$

and use

$$\int_{-\infty}^{\infty} \frac{\exp(-z^2)}{\sqrt{\pi}} dz = 1, \quad \int_{-\infty}^{\infty} \frac{z \exp(-z^2)}{\sqrt{\pi}} dz = 0, \quad \int_{-\infty}^{\infty} \frac{z^2 \exp(-z^2)}{\sqrt{\pi}} dz = \frac{1}{2},$$

so that (5.6) becomes

$$0 = dt + \varepsilon^2 \left(bu_x + \frac{1}{4}u_{xx} \right)$$

or

$$1 + f(x)u_x + \frac{\sigma^2(x)}{2}u_{xx} = 0.$$

For a similar derivation of the Fokker–Planck equation with variable diffusivity $\sigma(x)$, see the appendix in [17].

REFERENCES

- [1] Y. CHEN, T. KOLOKOLNIKOV, J. TZOU, AND C. GAI, *Patterned vegetation, tipping points, and the rate of climate change*, European J. Appl. Math., 26 (2015), pp. 945–958.
- [2] C. W. GARDINER, *Handbook of Stochastic Methods*, 3rd ed., Springer, Berlin, 1985.
- [3] A. GIERER AND H. MEINHARDT, *A theory of biological pattern formation*, Kybernetik, 12 (1972), pp. 30–39.
- [4] D. M. HOLLOWAY AND L. G. HARRISON, *Order and localization in reaction-diffusion pattern*, Phys. A, 222 (1995), pp. 210–233.
- [5] D. IRON AND M. J. WARD, *The dynamics of multispikes solutions to the one-dimensional Gierer–Meinhardt model*, SIAM J. Appl. Math., 62 (2002), pp. 1924–1951.
- [6] D. IRON, M. J. WARD, AND J. WEI, *The stability of spike solutions to the one-dimensional Gierer–Meinhardt model*, Phys. D, 150 (2001), pp. 25–62.
- [7] M. ISHIKAWA AND K. MIYAJIMA, *Analyses of pattern formation processes in stochastic activator-inhibitor systems with saturation in growth domains*, in Proceedings of the ISCIIE International Symposium on Stochastic Systems Theory and Its Applications, 2005, pp. 38–43.
- [8] J. P. KEENER, *A geometrical theory for spiral waves in excitable media*, SIAM J. Appl. Math., 46 (1986), pp. 1039–1056.
- [9] J. KELKEL AND C. SURULESCU, *On a stochastic reaction–diffusion system modeling pattern formation on seashells*, J. Math. Biol., 60 (2010), pp. 765–796.
- [10] T. KOLOKOLNIKOV AND J. WEI, *Pattern formation in a reaction-diffusion system with space-dependent feed rate*, SIAM Rev., 60 (2018), pp. 626–645.
- [11] T. KOLOKOLNIKOV AND S. XIE, *Spike density distribution for the gierer–meinhardt model with precursor*, Phys. D, (2019), 132247.
- [12] F. LI AND L. XU, *Finite time blowup of the stochastic shadow gierer-meinhardt system*, Electron. Commun. Probab., 20 (2015).
- [13] A. MUNTEANU AND R. V. SOLÉ, *Pattern formation in noisy self-replicating spots*, Internat. J. Bifurcation Chaos, 16 (2006), pp. 3679–3685.
- [14] J. D. MURRAY, *Mathematical Biology. II Spatial Models and Biomedical Applications*, Interdiscip. Appl. Math. 18, Springer, New York, 2001.
- [15] S. REDNER, *A Guide to First-Passage Processes*, Cambridge University Press, New York, 2001.
- [16] L. J. SCHUMACHER, T. E. WOOLLEY, AND R. E. BAKER, *Noise-induced temporal dynamics in turing systems*, Phys. Rev. E, 87 (2013), 042719.
- [17] J. SMITH-ROBERGE, D. IRON, AND T. KOLOKOLNIKOV, *Pattern formation in bacterial colonies with density-dependent diffusion*, European J. Appl. Math., 30 (2019), pp. 196–218.
- [18] G.-Q. SUN, L. LI, Z. JIN, AND B.-L. LI, *Effect of noise on the pattern formation in an epidemic model*, Numer. Methods Partial Differential Equations, 26 (2010), pp. 1168–1179.
- [19] J. WEI AND M. WINTER, *On the Gierer–Meinhardt system with precursors*, Discrete Contin. Dyn. Syst., 25 (2009).
- [20] J. WEI AND M. WINTER, *Mathematical Aspects of Pattern Formation in Biological Systems*, Dyn. Syst. Differential Equations 189, Springer, New York, 2013.

- [21] M. WINTER AND H. A. SHITU, *On Gierer-Meinhardt Model with Diffusion Constant of Mean Reverting Process Type*, preprint.
- [22] M. WINTER, L. XU, J. ZHAI, AND T. ZHANG, *The dynamics of the stochastic shadow Gierer–Meinhardt system*, *J. Differential Equations*, 260 (2016), pp. 84–114.